ELSEVIER

International Journal of Mass Spectrometry 185/186/187 (1999) 639–649

International Journal of Mass Spectrometry

Metastable states of dimethylsulfonium radical, $(CH_3)_2SH^{\cdot}$: a neutralization–reionization mass spectrometric and ab initio computational study

Martin Sadílek, František Tureček*

Department of Chemistry, Bagley Hall, University of Washington, Box 351700, Seattle, WA 98195-1700, USA

Received 24 June 1998; accepted 6 August 1998

Abstract

Variable-time neutralization–reionization mass spectrometry was used to generate and detect the hypervalent radical dimethylsulfonium, $(CH_3)_2SH^{\cdot}$ (**1H**$^{\cdot}$), and its isotopomers $(CH_3)_2SD^{\cdot}$ (**1HD**$^{\cdot}$), $(CD_3)_2SH^{\cdot}$ (**1DH**$^{\cdot}$), and $(CD_3)_2SD^{\cdot}$ (**1DD**$^{\cdot}$). The successful detection of **1H**$^{\cdot}$ **–1DD**$^{\cdot}$ was achieved in spite of severe interferences due to isobaric overlaps by the ^{13}C, ^{33}S, and ^{34}S isotope satellites of residual dimethylsulfide cation radicals. Radicals **1H**$^{\cdot}$ **–1DD**$^{\cdot}$ dissociated by cleavages of the S–(H,D) and S–C bonds in a ~3:1 branching ratio. Ab initio calculations with large basis sets failed to find a local energy minimum for the $(X)^2A'$ ground electronic state of **1H**$^{\cdot}$, which dissociated without barrier to $(CH_3)_2S$ and H$^{\cdot}$. Several excited states of **1H**$^{\cdot}$ were found by configuration interaction singles CIS/6-311++G(3*df*,2*p*) calculations that were within 2 eV of the repulsive ground state potential energy surface. The microsecond metastability and dissociations of **1H**$^{\cdot}$**–1DD**$^{\cdot}$ were ascribed to the properties of excited electronic states. (Int J Mass Spectrom 185/186/187 (1999) 639–649) © 1999 Elsevier Science B.V.

Keywords: Neutralization-reionization mass spectrometry; Dimethylsulfonium; Hypervalent radicals; Excited states; Ab initio calculations

1. Introduction

We have been interested in the gas-phase chemistry of hypervalent radicals of the onium type, e.g. ammonium, $R_4N^{\cdot}$, oxonium, $R_3O^{\cdot}$, and sulfonium, $R_3S^{\cdot}$ [1–13]. Hypervalent radicals represent a group of transient species that have been considered as intermediates of radical substitution reactions [14], one-electron reduction of onium cations [15,16], electrical discharge in gases [17], and dissociative electron-ion recombination [18,19]. A common feature of onium radicals is that they have extremely short lifetimes that prevent their detection in the condensed phase. In contrast, several hypervalent radicals have been generated by femtosecond collisional electron transfer in the gas phase [20–31] and studied by neutralization–reionization mass spectrometry (NRMS) [32] and ab initio calculations [33]. Precursor cations for hypervalent radicals are prepared conveniently by gas-phase protonation (chemical ionization) or fast-atom bombardment [31].

The previous studies showed that some hypervalent ammonium radicals existed in shallow potential energy minima and survived for several microseconds

* Corresponding author. E-mail: turecek@chem.washington.edu

Dedicated to Professor Michael T. Bowers on the occasion of his 60th birthday.

PII S1387-3806(98)14147-7

of flight time in the mass spectrometer. Such hypervalent radicals can be denoted as *metastables* [12], because their stabilities are due to potential energy barriers to exothermic dissociations by simple bond cleavages [2,9,35]. The kinetic stabilities of hypervalent radicals in their ground electronic states were found to decrease with increasing electron densities at the central heteroatom, e.g. in the series $NH_4^{\cdot} > CH_3NH_3^{\cdot} > (CH_3)_2NH_2^{\cdot} > (CH_3)_3NH^{\cdot}$ [2,9,35]. Hypervalent oxonium and sulfonium radicals, e.g. $(CH_3)_2OH^{\cdot}$ and $H_3S^{\cdot}$, were calculated to be unbound in their ground electronic states [4,7]. However, in spite of theoretical predictions, metastable hypervalent oxonium and sulfonium radicals of microsecond lifetimes have been observed experimentally in the gas phase [4,7,23,26–30]. The existence of these metastable radicals has been attributed to long-lived excited electronic states produced by collisional electron transfer [4,7,13]. The excited states in metastable hypervalent radicals have been probed by laser photoionization and photoexcitation for ND_4 [5] $(CH_3)_2OD^{\cdot}$ [7] and $(CH_3)_2ND_2^{\cdot}$ [9].

Amongst hypervalent onium radicals, sulfonium radicals represent a particular challenge to experimental and theoretical studies. The presence of stable sulfur isotopes introduces the possibility of isobaric overlaps between ^{32}S–^{1}H or ^{32}S–^{2}H species from the sulfonium ions and ^{33}S and ^{34}S species, respectively, from the residual thiol or sulfide cation radicals. The latter ions usually have substantially greater cross sections for collisional electron transfer than do the sulfonium ions and therefore can become unwanted contaminants in NR mass spectra. In addition, computational studies of $H_3S^{\cdot}$ [36] and other sulfur-centered radicals [37,38] revealed substantial basis set effects that made predictions of radical stabilities very difficult.

In the present work we address the question of metastability in the dimethylsulfonium radical, $(CH_3)_2SH^{\cdot}$ (**1H**$^{\cdot}$) (Scheme 1). Variable-time NR mass spectra are used to investigate the formation and dissociations of radical **1H**$^{\cdot}$ and its deuterium-labeled derivatives **1HD**$^{\cdot}$, **1DH**$^{\cdot}$, and **1DD**$^{\cdot}$. Configuration-interaction singles (CIS) ab initio calculations [39] with large basis sets are used to probe the electronic states of **1H**$^{\cdot}$.

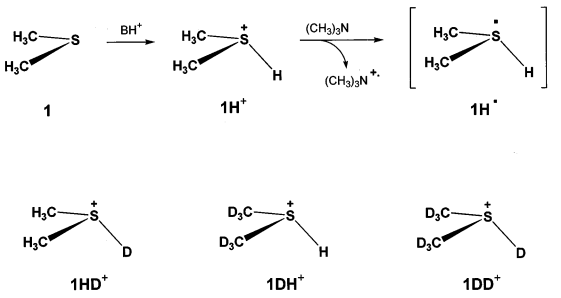

Scheme 1

2. Experimental

2.1. Materials

Dimethylsulfide was purchased from Aldrich Chemical Co. (Milwaukee, WI) and purified by several freeze–pump–thaw cycles before use. Di-(methyl-d_3)sulfide was prepared by reduction of dimethylsulfoxide-d_6 (Cambridge Laboratories, Andover, MA, 99.9% D) using a literature procedure [40]. The product was purified by distillation and degassed by several freeze–pump–thaw cycles before use. The other materials were isobutane (Matheson, 99.5%), methane (Matheson, 99.9%), acetone and methanol (HPLC grade, Fisher), acetone-d_6 and methanol-d_4 (Cambridge Laboratories, Andover, MA, 99.9% D).

2.2. Methods

Measurements were made on a tandem quadrupole acceleration–deceleration mass spectrometer described previously [41]. Chemical ionization with CH_5^+ /CH_4, $CH_3OH_2^+$/CH_3OH, t-$C_4H_9^+$/i-C_4H_{10}, and $(CH_3)_2C$-OH^+/acetone was used to generate dimethylsulfonium ions (**1H**$^+$) and di-(methyl-d_3)sulfonium ions **1DH**$^+$. $CD_3OD_2^+$/CD_3OD and $(CD_3)_2C$–OD^+/$(CD_3)_2C{=}O$ were used for deuteronation to prepare ions **1HD**$^+$ and **1DD**$^+$. Chemical ionization (CI) was performed in a tight ion source of our design and care

was taken to achieve high conversion to protonated or deuteronated ions in order to minimize formation of dimethylsulfide cation radicals. The collisional conditions were as follows. The ion kinetic energy was adjusted to 8200–8230 eV; trimethylamine and oxygen were used as neutralization and reionization gases, respectively, at pressures allowing 70% transmittance (T) of the precursor ion beam.

Variable-time measurements were performed in a 60-cm-long drift region between the neutralization and reionization cells using a system of floated cylindrical lenses as described previously [42,43]. Briefly, a combination of fixed (+250 V) and scanned (from 0 to −8230 V) voltages was applied to the lenses to create an observation window for ions formed by collisional reionization. Only ions with a correct combination of mass, potential, and kinetic energy were able to pass through an energy filter and the quadrupole mass analyzer and be detected. The total flight time through the drift region was kept constant (t), while the lengths of the observation windows were varied stepwise to achieve flight times for the neutral species (t_N) and reionized ions (t_i) such that $t = t_N + t_i$. The observation times for $\mathbf{1H}^{\cdot}$ dissociations were 0.35, 1.05, 1.76, 2.47, and 3.78 μs. The observation times for $\mathbf{1H}^{+}$ dissociations were 3.44, 2.73, 2.02, and 1.31 μs. The observation times for the labeled radicals and ions (X) were longer proportionately to $[(m/z = X)/(m/z = 63)]^{1/2}$, e.g. 0.37, 1.11, 1.86, 2.60, and 3.98 μs for $\mathbf{1DD}^{\cdot}$ of $m/z = 70$, and likewise for the others.

2.3. Calculations

Standard ab initio calculations were carried out with the GAUSSIAN 94 set of programs [44]. Ion and neutral geometries were optimized with perturbational Moller–Plesset calculations, MP2(FULL), using the 6-31++G(2d,p) basis set furnished with a split set of polarization functions and *sp* shells of diffuse functions on heavy atoms and hydrogens. Zero-point energies and thermal corrections were taken from previously published data [45]. Single-point energies were calculated with MP2(frozen core) using the larger 6-311++G(3df,2p) basis set. Geometry optimizations of $\mathbf{1H}^{\cdot}$ were also carried out with density functional theory calculations that used Becke's three parameter hybrid functional (B3LYP) [46], which includes a local correction functional by Vosko et al. [47] and a nonlocal correction by Lee et al. [48]. These calculations used the 6-311++G(2df,2p) basis set. Excited state energies were calculated with the CIS method [39]. Geometry optimizations of excited states were conducted with CIS/6-31++G(2d,p). Single-point energies for several excited electronic states were calculated with CIS/6-311++G(3df,2p).

Table 1
Proton affinities and protonation exothermicities for the formation of $\mathbf{1H}^{+}$

Reagent gas/acid	PA[a] (kJ mol^{-1})	ΔPA[b]
CH_4/CH_5^+	544	287
H_2O/H_3O^+	691	140
$CH_3OH/CH_3OH_2^+$	754	77
2-methylpropene/t-$C_4H_9^+$	802	29
2-propanone/$(CH_3)_2C{-}OH^+$	812	19
dimethylsulfide/$CH_3SCH_3^{+\cdot}$	831	−47[c]

[a] In kJ mol^{-1}.
[b] Protonation exothermicity for the formation of $(CH_3)_2S{-}H^+$.
[c] For the reaction: $CH_3SCH_3^{+\cdot} + (CH_3)_2S \rightarrow CH_3SCH_2^{\cdot} + (CH_3)_2S{-}H^+$.

3. Results and discussion

3.1. Neutral dissociations

Precursor ions for the formation of $\mathbf{1H}^{\cdot}$ were prepared by protonation of dimethylsulfide **(1)** with gas-phase acids having a wide range of acidities (Table 1). Based on the revised proton affinity of **1** (831 kJ mol^{-1} [49,50]) protonations with CH_5^+ through self-CI with $CH_3SCH_3^{+\cdot}$ ranged from 287 kJ mol^{-1} exothermic to 47 kJ mol^{-1} endothermic. Self-CI of **1** produced mostly the dimer, $(CH_3)_2S^{+\cdot}{:}S(CH_3)_2$ (100% relative abundance), whereas protonation was much less efficient (10%). The formation of $\mathbf{1H}^{+}$ under self-CI conditions must be due to the presence of high-energy $\mathbf{1}^{+\cdot}$ from 100 eV electron-impact ionization or it may be caused by ion fragments of PA smaller than that of **1**. Neutralization of

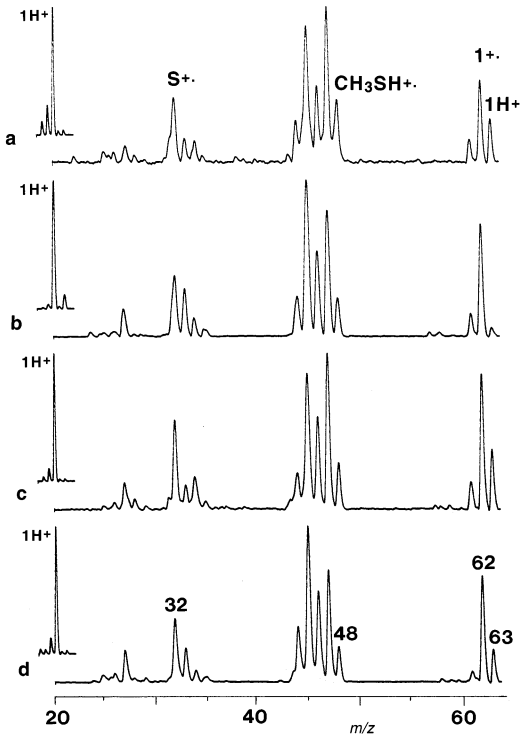

Fig. 1. NR mass spectra [$(CH_3)_3N$, 70% transmittance/O_2, 70% transmittance] of $\mathbf{1H^+}$ prepared by protonation with (a) CH_5^+, (b) $CH_3OH_2^+$, (c) t-$C_4H_9^+$, (d) $(CH_3)_2C$–OH^+. Insets show the m/z = 60–67 groups for $\mathbf{1H^+}$ from chemical ionization.

$\mathbf{1H^+}$ with trimethylamine followed by reionization with oxygen gave the spectra shown in Fig. 1. The intermediate radicals $\mathbf{1H^{\cdot}}$ dissociated by loss of $H^{\cdot}$ to give **1**, which was detected after ionization at m/z = 62. Likewise, loss of methyl gave rise to CH_3SH which gave a peak at m/z = 48 following reionization. These dissociations correspond to S–H and S–C bond cleavages at the hypervalent sulfur atom. The neutral products, CH_3SH and **1**, are stable molecules which are not expected to dissociate. For example, the S–C bond dissociation energies in **1** and CH_3SH are 307–308 kJ mol^{-1}, and the S–H bond dissociation energy in the latter molecule is 364 kJ mol^{-1} [51].

The branching ratios for [$\mathbf{1H^{\cdot}}$–H]/[$\mathbf{1H^{\cdot}}$–CH_3] were estimated from [12]

$$[\mathbf{1H^{\cdot}}\text{–H}]/[\mathbf{1H^{\cdot}}\text{–}CH_3] = \{I(m/z = 62)/I(m/z = 48)\} \times [I_{rel}\mathbf{(1)}\sigma(CH_3SH)]/I_{rel}(CH_3SH)\sigma\mathbf{(1)}] \quad (1)$$

$$\Sigma I_{NR}(CH_3SH) = F(CH_3SH) \times Nl\sigma(CH_3SH) \quad (2)$$

$$I_{rel}(CH_3SH)^{+\cdot} = I_{NR}(CH_3SH)^{+\cdot}/\Sigma I_{NR}(CH_3SH) \quad (3)$$

where $I(m/z = 62)$ and $I(m/z = 48)$ are the integrated intensities (areas) of the corresponding signature peaks in the NR spectrum of $\mathbf{1H^+}$, I_{rel} are the relative intensities of the corresponding ions in the reference NR spectra of [$\mathbf{1}^{+\cdot}$] and [$CH_3SH^{+\cdot}$], respectively, and σ are the corresponding ionization cross sections. Eq. (1) relies on Eqs. (2) and (3) (shown for CH_3SH only), which relate the neutral flux F of each species to its total NR ion current ΣI_{NR}, ionization cross section σ, number density of the reionization gas N, path length l, and relative intensity of the signature ion I_{rel} in the reference spectrum. The ionization cross sections were estimated from the additive scheme of Fitch and Sauter [52] as σ = 7.5 and 9.7 × 10^{-16} cm^2 for CH_3SH and **1**, respectively. Note, that only the relative value, $\sigma(CH_3SH)/\sigma\mathbf{(1)}$, is needed in Eq. (1).

The branching ratios showed no clear trends depending on the internal energy of the precursor ion or observation time for neutral dissociations. For example, precursor ions $\mathbf{1H^+}$ were prepared by protonation with CH_5^+, $CH_3OH_2^+$, t-$C_4H_9^+$, and $(CH_3)_2C$–OH^+ of decreasing exothermicity. The respective [$\mathbf{1H^{\cdot}}$–H]/[$\mathbf{1H^{\cdot}}$–CH_3] branching ratios for the radical dissociations were 66/34, 74/26, 69/31, and 73/27. For the least exothermic ionization with $(CH_3)_2C$–OH^+, the [$\mathbf{1H^{\cdot}}$–H]/[$\mathbf{1H^{\cdot}}$–CH_3] branching ratios were 76/24, 77/23, 70/30, and 73/27 (all ±3%) for radicals dissociating within 0.35, 1.05, 1.76, and 2.47 μs, respectively. Clearly, cleavages of both the S–H and S–CH_3 bonds took place in hypervalent radicals $\mathbf{1H^{\cdot}}$ but were insensitive to the radicals' internal energy or lifetime.

Dissociations of deuterium-labeled radicals $\mathbf{1DH^{\cdot}}$, $\mathbf{1HD^{\cdot}}$, and $\mathbf{1DD^{\cdot}}$ also showed cleavages of S–H, S–D, S–CH_3, and S–CD_3 bonds [Figs. 2(a)–(c)]. The branching ratios for the various combinations of nonlabeled and labeled products, CD_3SH, CH_3SD, $(CH_3)_2S$, and $(CD_3)_2S$, were not established because of lack of suitable reference spectra. Note that the I_{rel} values in Eq. (3) may be affected by isotope effects on dissociations of labeled reionized products. Deute-

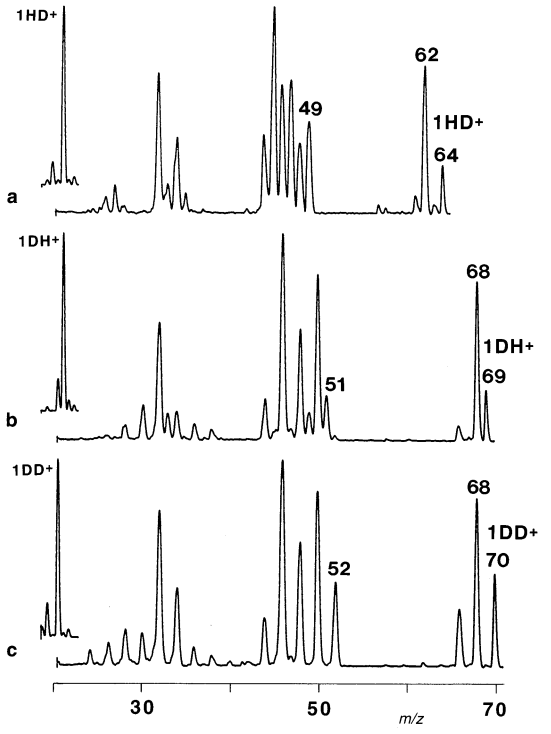

Fig. 2. NR mass spectra [$(CH_3)_3N$, 70% transmittance/O_2, 70% transmittance] of (a, top) **1HD**$^+$ from deuteronation of **1** with $(CD_3)_2C–OD^+$, (b, middle) **1DH**$^+$ from protonation of **1D** with $(CH_3)_2C–OH^+$, and (c, bottom) **1DD**$^+$ from deuteronation of **1D** with $(CD_3)_2C–OD^+$.

rium isotope effects in NR spectra have been noted previously [9,28,30]. However, the NR spectra indicated preferential cleavages of S–(H,D) bonds in hypervalent radicals **1DH**$^\cdot$, **1HD**$^\cdot$, and **1DD**$^\cdot$.

3.2. Metastable radicals

The NR spectra of dimethylsulfonium ions showed peaks at mass-to-charge ratio values corresponding to survivor ions for **1H**$^\cdot$ [Fig. 1(a)–(d)] **1HD**$^\cdot$ [Fig. 2(a)], **1DH**$^\cdot$ [Fig. 2(b)], and **1DD**$^\cdot$ [Fig. 2(c)]. However, the identity of these ions may be compromised by isobaric overlaps of, for example, **1H**$^+$ with the ^{13}C and ^{33}S isotopomers of **1**$^{+\cdot}$, or **1D**$^+$ with the ^{34}S isotopomer of **1**$^{+\cdot}$. How severe this problem can be is shown in Fig. 3. The m/z = 60–65 ion group from protonation with CH_5^+ showed a 12/100 ratio of

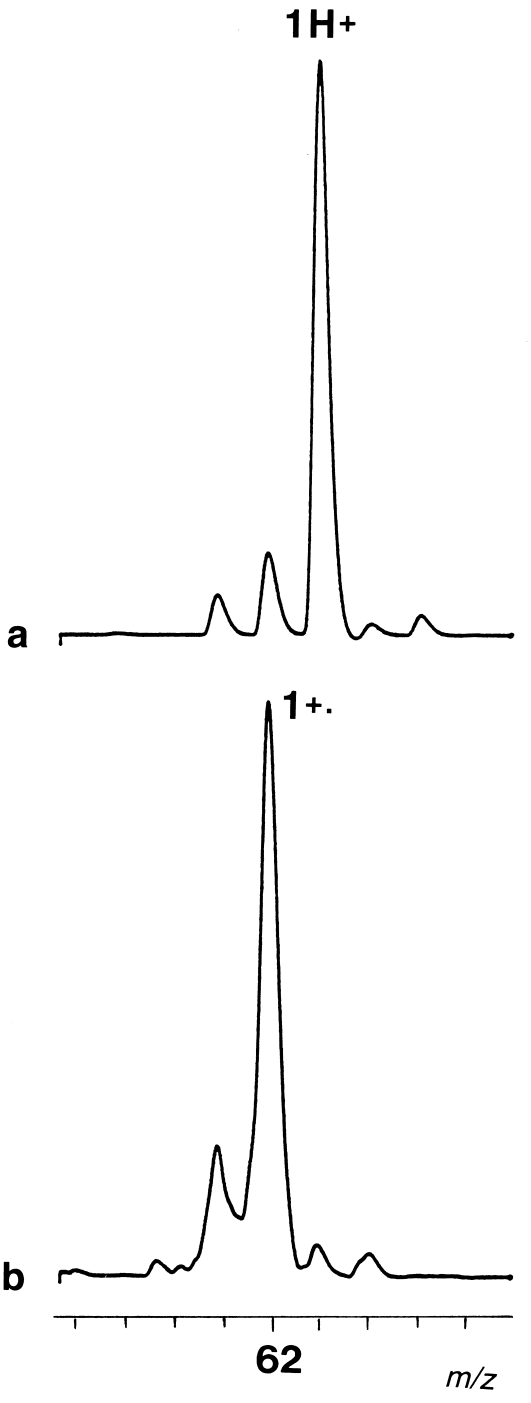

Fig. 3. CI mass spectrum (a, top) and survivor-ion NR mass spectrum [$(CH_3)_3N$, 70% transmittance/O_2, 70% transmittance] (b, bottom) of the m/z = 58–67 group from protonation of **1** with CH_5^+.

$[\mathbf{1}^{+\cdot}]/[\mathbf{1H}^{+}]$ [Fig. 3(a)], corresponding to only 0.4% of combined ^{13}C and ^{33}S isotopomers overlapping with $\mathbf{1H}^{+}$ at $m/z = 63$. However, the survivor-ion spectrum [53] of this ion group showed mostly $\mathbf{1}^{+\cdot}$ at $m/z = 62$ and its isotope satellites at $m/z = 63$ and 64. The contribution of survivor $\mathbf{1H}^{+}$ at $m/z = 63$ was only 3% of the survivor $\mathbf{1}^{+\cdot}$ when corrected for the ($^{13}C + {}^{33}S$) isotope satellites of the latter [Fig. 3(b)]. This implied that the NR efficiency for producing survivor $\mathbf{1H}^{+}$ relative to that of $\mathbf{1}^{+\cdot}$, $f_{rel} = (12/100)/(100/3) = 0.0036$, was very small, and the NR formation of $\mathbf{1}^{+\cdot}$ was 278 times more efficient than $\mathbf{1H}^{+}$. Hence, the presence of low-level isotope satellites of residual $\mathbf{1}^{+\cdot}$ is expected to cause large variations in the relative intensity of survivor ions in standard NR spectra.

Fortunately, this large background effect can largely be removed by exploiting the different time dependence of the $\mathbf{1}^{+\cdot}$ and $\mathbf{1H}^{+}$ ion intensities in variable-time NR spectra. The variable-time spectra of $\mathbf{1}^{+\cdot}$ showed that the relative intensities of survivor ions $[\mathbf{1}^{+\cdot}]$ slightly decreased when the time window for ion dissociations was increased while the time window for neutral dissociations was decreased. For example, $[\mathbf{1}^{+\cdot}]$ was 47 and 44% ΣI_{NR} (both ±1%) at neutral lifetimes of 3.75 μs and 0.35, respectively. The effect of neutral and ion lifetimes practically disappeared for $\mathbf{1}^{+\cdot}$ prepared by charge–exchange ionization with $C_6D_6^{+\cdot}$, which is exoergic by mere $\Delta IE = 0.56$ eV and in which ions $\mathbf{1}^{+\cdot}$ can be further thermalized in the ion source by collisions with excessive C_6D_6 molecules. The $[\mathbf{1}^{+\cdot}]$ from the variable-time NR spectra were 50 ± 1% for 0.35 and 3.75 μs neutral dissociation windows. Effects of neutral and ion lifetimes were also observed for dissociations of $\mathbf{1D}^{+\cdot}$ which gave 33% and 42% of surviving $\mathbf{1D}^{+\cdot}$ at neutral lifetimes of 0.37 and 3.93 μs. It can be concluded from these variable-time measurements that neutralization of $\mathbf{1}^{+\cdot}$ and its isotopomers did not result in neutral dissociations. The fragments observed in the NR spectra originated from ion dissociations induced by collisional reionization.

Variable-time spectra were obtained for hypervalent radicals $\mathbf{1H}^{\cdot}$ (Fig. 4), $\mathbf{1HD}^{\cdot}$, $\mathbf{1DH}^{\cdot}$, and $\mathbf{1DD}^{\cdot}$ (Fig. 5). The spectra of $\mathbf{1H}^{\cdot}$ showed decreasing relative

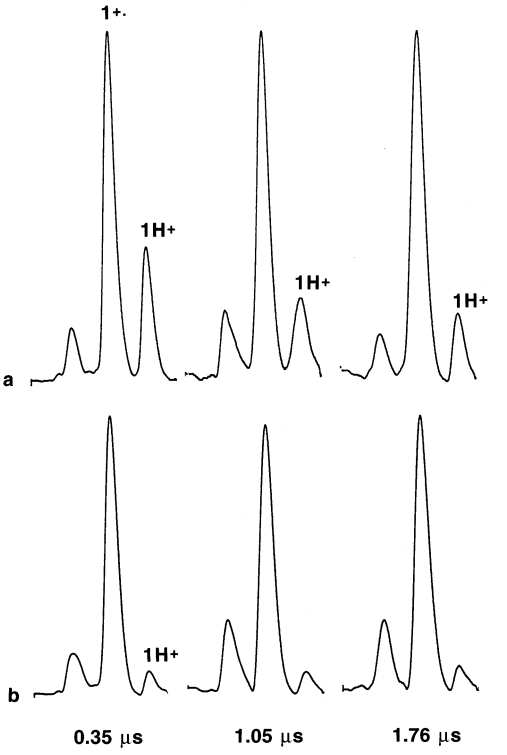

Fig. 4. Variable-time NR mass spectra of $\mathbf{1H}^{+}$ from (a, top) protonation with $(CH_3)_2C–OH^{+}$, (b, bottom) protonation with $CH_3OH_2^{+}$. NR conditions as in Fig. 1.

abundances of survivor $\mathbf{1H}^{+}$ upon increasing the observation time for neutral dissociations. For example, for $\mathbf{1H}^{+}$ prepared by mildly exothermic protonation with $(CH_3)_2C–OH^{+}$, the $[\mathbf{1H}^{+}]/[\mathbf{1}^{+\cdot}]$ ratio decreased from 0.36 at 0.35 μs neutral lifetime to 0.15 at 1.76 μs [Fig. 4(a)]. This effect pointed clearly to a fraction of *metastable* $\mathbf{1H}^{\cdot}$ dissociating on the microsecond time scale. Note that isobaric contaminants due to ^{13}C and ^{33}S isotopomers of $\mathbf{1}^{+\cdot}$ would have shown a *weak and opposite* trend, similar to that observed for $\mathbf{1}^{+\cdot}$. The existence of metastable $\mathbf{1H}^{\cdot}$ was thus proven free of interferences. In contrast, neutralization of $\mathbf{1H}^{+}$ from protonation with $CH_3OH_2^{+}$ showed variable fractions of survivor $\mathbf{1H}^{\cdot}$ that depended on the reagent gas pressure in the ion source. For low pressures of methanol, the variable-time NR spectra indicated the presence of survivor $\mathbf{1H}^{\cdot}$ in spite of contamination with (^{13}C, ^{33}S)$\mathbf{1}^{+\cdot}$. For high pres-

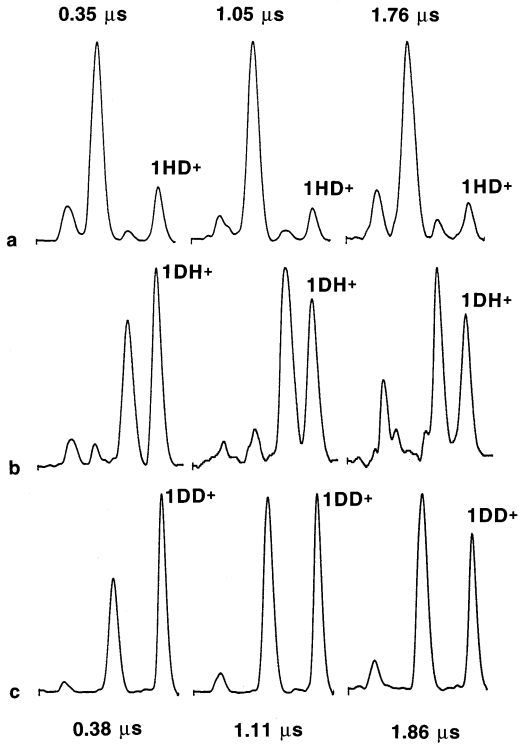

Fig. 5. Variable-time NR mass spectra of (a, top) **1HD**$^+$ from deuteronation of **1** with $(CD_3)_2C–OD^+$; (b, middle) **1DH**$^+$ from protonation of **1D** with $(CH_3)_2C–OH^+$; (c, bottom) **1DD**$^+$ from deuteronation of **1D** with $(CD_3)_2C–OD^+$. NR conditions as in Fig. 1.

sures of methanol, the survivor ion practically disappeared [Fig. 4(b)]. In addition, the weak dependence on the neutral lifetime of the survivor ion intensity indicated that the ion was mostly composed of residual (^{13}C, ^{33}S)**1**$^{+\cdot}$. Similar effects of source pressure on hypervalent radical stabilities have been observed previously for oxonium radicals [28–30]. A detailed analysis for $H_3S^{\cdot}$ [4] indicated that the pressure effect may be due to hyperthermal vibrational energies of precursor onium ions prepared by highly exothermic protonation at low pressures. Collisional neutralization of vibrationally excited ions forms fractions of hypervalent radicals in bound excited electronic states. It is not clear at present whether the vibrational excitation in the precursor ion increases the Franck–Condon overlaps for electron transfer into the excited state, or whether vibrational excitation in the bound radical excited state decreases the transition moment for radiative transition to the weakly bound or unbound ground electronic state. Studies towards this end are underway [54].

The deuterium-labeled radicals also showed substantial fractions of survivor ions that were distinguished from isobaric interferences by variable-time NR spectra. Effects of neutral lifetimes were observed for **1HD**$^{\cdot}$ generated by neutralization of **1HD**$^+$; the latter was prepared by exothermic deuteronation with $CD_3OD_2^+$ at low ion source pressure. The variable time spectra [Fig. 5(a)] showed that the relative abundance of survivor **1HD**$^+$ decreased with increasing observation time for neutral dissociations. The corresponding [**1HD**$^+$]/[**1**$^{+\cdot}$] abundance ratios were 0.22, 0.14, and 0.13 for neutral lifetimes of 0.35, 1.05, and 1.76 μs, respectively. **1DH**$^{\cdot}$ from protonation of **1D** with $(CH_3)_2C–OH^+$ gave variable-time spectra that showed fractions of survivor ions at m/z = 69 that decreased with increasing the observation time for neutral dissociations from 0.38 to 1.84 μs [Fig. 5(b)]. The changes were substantial, e.g. the [**1DH**$^+$]/[**1D**$^{+\cdot}$] = 1.13, 0.71, and 0.62 at neutral lifetimes of 0.38, 1.10, and 1.84 μs, respectively. Conspicuous changes in the relative abundance of **1DD**$^+$ were also observed in the variable time spectra shown in Fig. 4(c). The survivor ion relative abundance was measured as [**1DD**$^+$]/[**1D**$^{+\cdot}$] = 1.37, 0.83, and 0.63 at neutral lifetimes of 0.38, 1.11, and 1.86 μs, respectively.

3.3. Neutral structures and energies

The variable-time measurements clearly indicated that metastable hypervalent radicals **1H**$^{\cdot}$, **1HD**$^{\cdot}$, **1DH**$^{\cdot}$, and **1DD**$^{\cdot}$ of microsecond lifetimes were formed by collisional electron transfer. However, these measurements did not provide data on the structure and energetics of the species under study. Structures and energies were therefore obtained by ab initio calculations. Geometry optimizations of radical **1H**$^{\cdot}$ started from the optimized geometry of ion **1H**$^+$ (Fig. 6) and several other initial geometries of different S–H bonds. In each case, the calculations showed large initial negative gradients along the S–H coordinate

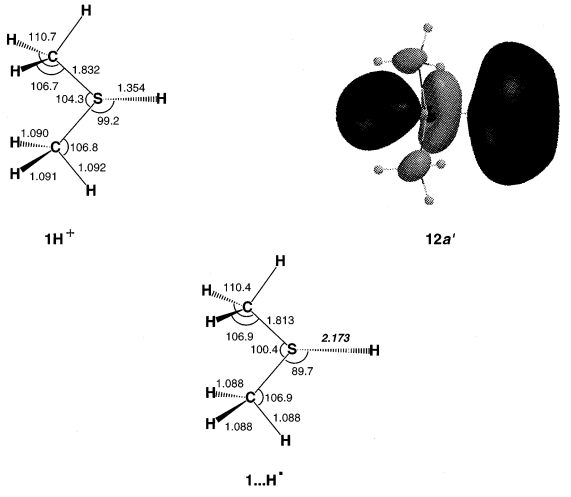

Fig. 6. The 12a' singly occupied molecular orbital (SOMO) in vertically formed **1H**$^{\cdot}$ from UHF/6-311++G(2d,p) orbital analysis and the B3LYP/6-311++G(2df,2p) optimized structure of the (**1** + H)$^{\cdot}$ complex.

and resulted in dissociation to **1** and hydrogen atom. Additional geometry optimizations were attempted by using density functional theory (DFT) and the larger 6-311++G(2df,2p) basis set. This basis set was deemed to be sufficiently flexible to handle even weak, long bonds in hypervalent radicals [4,7]. DFT methods, e.g. those using Becke's hybrid functional (B3LYP) tend to slightly overstabilize radicals [55], which was thought to be helpful in finding a potential energy minimum for ground-state **1H**$^{\cdot}$. A geometry optimization with B3LYP/6-311++G(2df,2p) resulted in an exothermic dissociation of the S–H bond. A shallow local energy minimum was found which showed a long S–H bond (2.173 Å, Fig. 6) in a loose complex of **1** and a hydrogen atom which was bound by mere 4 kJ mol^{-1} at 0 K, which increased to 7 kJ mol^{-1} at 298 K. However, a single point calculation with spin projected MP2/6-311++G(3df,2p) placed the respective 0 and 298 K energies of the **1** . . . H$^{\cdot}$ complex at 13 and 10 kJ mol^{-1} *above* the products. Hence, the existence of a weak complex of **1** and a hydrogen atom was not established unambiguously even at the present high level of theory.

By comparison, $(X)^2A'$**1H**$^{\cdot}$ formed by vertical neutralization of ion **1H**$^+$ was calculated by B3LYP/6-311++G(2df,2p) and UMP2/6-311++G(3df,2p), respectively, to be 78–137 kJ/mol^{-1} above the energy of the dissociation products, **1** + H$^{\cdot}$. This means that regardless of the possible existence of a loosely bound complex along the dissociation path, the $(X)^2A'$ state of **1H**$^{\cdot}$ when formed by vertical electron transfer had a sufficient internal energy to dissociate by hydrogen atom loss. The instability of **1H**$^{\cdot}$ was in line with previous calculations of $H_3S^{\cdot}$ that also failed to find a bound structure at several levels of theory [4,36]. A qualitative rationalization of the weak S–H bond followed from the lobal properties of the 12a′ SOMO in vertically formed **1H**$^{\cdot}$ (Fig. 6). The SOMO was antibonding along the S–H bond and showed an unusually large spin density (+1.15) and a negative charge (−0.95) on the hydrogen atom. This accumulation of electron density on the hydrogen atom apparently contributed to the disruption of the S–H σ bond and increased the potential energy of **1H**$^{\cdot}$ high above the dissociation limit.

Vertical neutralization of **1H**$^+$ to the repulsive part of the $(X)^2A'$ ground-state potential energy surface of **1H**$^{\cdot}$ was accompanied with a recombination energy that was calculated by MP2/6-311++G(3df,2p) as RE_v = 3.70 eV. Vertically formed radical **1H**$^{\cdot}$ was calculated to dissociate exothermically to **1** + H$^{\cdot}$ (ΔH_r = −137 kJ mol^{-1}) and/or CH_3SH + $CH_3^{\cdot}$ (ΔH_r = −174 kJ mol^{-1}) (Fig. 7). The MP2-calculated difference in the product enthalpies (37 kJ mol^{-1} in favor of CH_3SH + $CH_3^{\cdot}$ at 298 K) was somewhat lower than the value from standard thermochemical data (58 kJ mol^{-1}) [51]. The thermochemical data thus preferred the formation of CH_3SH + CH_3 as the more exothermic channel. However, since vertically formed **1H**$^{\cdot}$ was unbound with respect to S–H bond cleavage, the latter dissociation must have occurred in a time shorter than the vibrational period for the S–H stretch. From the corresponding wave number in **1H**$^+$, ν(S–H) = 2558 cm^{-1}, the vibrational period was estimated as $t = 1.30 \times 10^{-14}$ s. This short lifetime was not only incompatible with the existence of metastable **1H**$^{\cdot}$, but also did not allow a competing S–CH_3 bond cleavage to occur provided the radical was bound along the S–C coordinate. The observed loss of methyl from **1H**$^{\cdot}$ was therefore difficult to

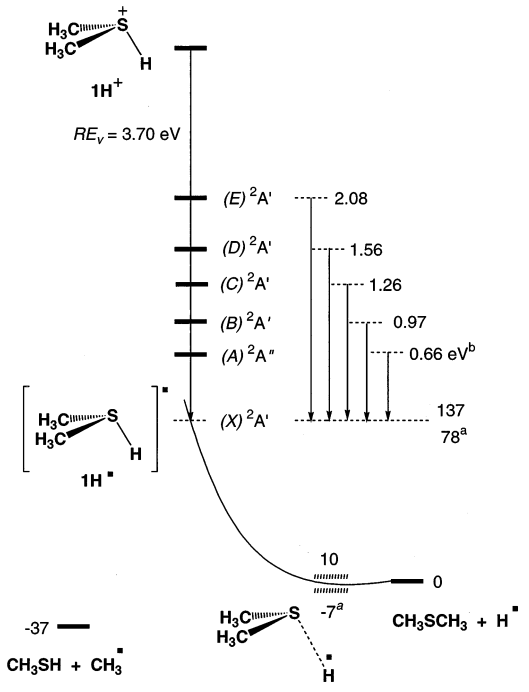

Fig. 7. Potential energy diagram for neutralization of $\mathbf{1H}^+$ and dissociations of $\mathbf{1H}^{\cdot}$. Energies in kJ mol^{-1} from MP2/6-311++G(3*df*,2*p*) calculations. (a) B3LYP/6-311++G(2*df*,2*p*) energies. (b) CIS/6-311++G(3*df*,2*p*) excitation energies in electron volts.

explain based on the properties of the ground-electronic state of $\mathbf{1H}^{\cdot}$ alone.

In the absence of a bound structure for ground-state $\mathbf{1H}^{\cdot}$, its metastability and dissociation by loss of methyl must be due to the population of excited electronic states. Electronic states in $\mathbf{1H}^{\cdot}$ were probed with CIS/6-311++G(3*df*,2*p*) single-point calculations for a nonequilibrium geometry corresponding to vertical electron capture, $\mathbf{1H}^+ \rightarrow \mathbf{1H}^{\cdot}$. The use of single excitations in the configuration interaction calculations was justified by the ordering of the molecular orbital energies in $\mathbf{1H}^{\cdot}$. The SOMO energy ($12a'$, $-\epsilon_{SOMO} = 3.30$ eV), which confines the energy span of the unoccupied orbitals, was substantially smaller than the excitation energy from the highest doubly occupied molecular orbital, $E(11a' \rightarrow 12a') = 9.85$ eV. Excitations in the CI procedure thus involved almost exclusively the $12a'$ electron and the manifold of unoccupied orbitals of appropriate symmetry.

Several excited states were identified by CIS/6-311++G(3*df*,2*p*) calculations, e.g. $(A)^2A''$, $(B)^2A'$, $(C)^2A'$, $D(^2A')$, and $E(^2A')$, which were within 2.0 eV of the point of vertical landing on the repulsive (X) state. The A, B, C, and E states showed moderately low oscillator strengths for radiative transition to the repulsive ground state, $f \leq 0.05$, which could possibly further decrease at geometries corresponding to local energy minima on the excited state potential energy surfaces. However, attempts to fully optimize with CIS/6-31++G(2*df*,*p*) the geometries for the (A) and (B) states were unsuccessful. The problem with the CIS gradient optimizations was that they produced unpredictable errors in virtual orbital selection to construct the CIS matrix. Although progress towards (possible) local minima at the (A) and (B) state potential energy surfaces had been made, the calculations became too expensive to be practical and had to be abandoned. Nevertheless, the not fully optimized structures showed slow convergence towards standard C–S and S–H bond lengths, e.g. 1.816 and 1.336 Å, respectively, for the (A) state, and 1.907 and 1.317 Å, respectively, for the (B) state, that indicated that local energy minima may exist on these potential energy surfaces. Simultaneously, the oscillator strengths for radiative transitions to the (X) state decreased below 0.02 for the (A) and (B) states. Although these partial optimizations are not conclusive, they may indicate the existence of long-lived, bound excited states in $\mathbf{1H}^{\cdot}$.

4. Conclusions

Variable-time neutralization–reionization measurements allowed us to distinguish long-lived hypervalent dimethylsulfonium radicals and their deuterium isotopomers even in the presence of substantial background due to isobaric overlaps. This added dimension in NRMS showed promise for the detection of extremely labile species and distinction of neutral and ionic dissociations even if they formed chemically identical products. Ab initio calculations indicated

that vertical neutralization of $\mathbf{1H}^+$ landed on a repulsive part of the $(X)^2A'$ potential energy surface of $\mathbf{1H}^{\cdot}$ so that the latter should dissociate within 10^{-14} s by cleavage of the S–H bond. The existence of metastable $\mathbf{1H}^{\cdot}$ and dissociations by S–C bond cleavage are tentatively ascribed to long-lived, bound excited electronic states that are populated by femtosecond collisional electron transfer. Ab initio calculations of excited electronic states in hypervalent sulfonium radicals are difficult and yet not fully conclusive.

Acknowledgements

Support by the National Science Foundation (grant no. CHE-9712570) is gratefully acknowledged. The computations were carried out at the University of Washington Computing and Communications Center and at the Chemistry Department Computer Cluster. The authors thank Jill K. Wolken for technical assistance.

References

[1] F. Tureček, Org. Mass Spectrom. 27 (1992) 1087.
[2] S.A. Shaffer, F. Tureček, J. Am. Chem. Soc. 116 (1994) 8647.
[3] S.A. Shaffer, F. Tureček, J. Am. Soc. Mass Spectrom. 6 (1995) 1004.
[4] M. Sadílek, F. Tureček, J. Phys. Chem. 100 (1996) 15027.
[5] M. Sadílek, F. Tureček, Chem. Phys. Lett. 263 (1996) 203.
[6] S.A. Shaffer, M. Sadílek, F. Turecek, J. Org. Chem. 61 (1996) 5234–5245.
[7] M. Sadílek, F. Tureček, J. Phys. Chem. 100 (1996) 9610–9614.
[8] S.A. Shaffer, M. Sadilek, F. Tureček, C.E.C.A. Hop, Int. J. Mass Spectrom. Ion Processes 160 (1997) 137.
[9] V.Q. Nguyen, M. Sadilek, A.J. Frank, J.G. Ferrier, F. Tureček, J. Phys. Chem. A 101 (1997) 3789.
[10] J.K. Wolken, V.Q. Nguyen, F. Tureček, J. Mass Spectrom. 32 (1997) 1162.
[11] S.A. Shaffer, J.K. Wolken, F. Tureček, J. Am. Soc. Mass Spectrom. 8 (1997) 1111.
[12] L. Frøsig, F. Tureček, J. Am. Soc. Mass Spectrom. 9 (1998) 242.
[13] F. Tureček, in Proceedings of the Seventh National Symposium on Mass Spectrometry, S.K. Aggarwal, H.C. Jain (Eds.), Indian Society for Mass Spectrometry, Defence Research and Development Establishment, Gwalior, India, 1996.
[14] C.W. Perkins, J.C. Martin, A.J. Arduengo, W. Lau, A. Alegria, J.K. Kochi, J. Am. Chem. Soc. 102 (1980) 7753.
[15] R.N. Gedye, Y.N. Sadana, J. Org. Chem. 45 (1980) 3721.
[16] E. Kariv-Miller, C. Nanjudiah, J. Eaton, K.E. Swenson, J. Electroanal. Chem. 167 (1984) 141.
[17] G. Herzberg, Faraday Discuss. R. Soc. Chem. 71 (1981) 165.
[18] D.R. Bates, in Dissociative Recombination, B.R. Rowe, J.B.A. Mitchell, A. Canosa (Eds.), NATO ASI Series, Plenum, New York, 1993, pp. 1–10.
[19] N.G. Adams, in Dissociative Recombination, B.R. Rowe, J.B.A. Mitchell, A. Canosa (Eds.), NATO ASI Series, Plenum, New York, 1993, pp. 99–112.
[20] B.W. Williams, R.F. Porter, J. Chem. Phys. 73 (1980) 5598.
[21] G.I. Gellene, D.A. Cleary, R.F. Porter, J. Chem. Phys. 77 (1982) 3471.
[22] S.-J. Jeon, A.B. Raksit, G.I. Gellene, R.F. Porter, J. Am. Chem. Soc. 107 (1985) 4129.
[23] W.J. Griffiths, F.M. Harris, J.H. Beynon, Int. J. Mass Spectrom. Ion Processes 77 (1987) 233.
[24] G.I. Gellene, R.F. Porter, J. Chem. Phys. 81 (1984) 5570.
[25] A.B. Raksit, S.-J. Jeon, R.F. Porter, J. Phys. Chem. 90 (1986) 2298.
[26] A.B. Raksit, R.F. Porter, J. Chem. Soc. Chem. Commun. (1987) 500.
[27] A.B. Raksit, R.F. Porter, Org. Mass Spectrom. 22 (1987) 410.
[28] J.L. Holmes, M. Sirois, Org. Mass Spectrom. 25 (1990) 481.
[29] M. Sirois, M. George, J.L. Holmes, Org. Mass Spectrom. 29 (1994) 11.
[30] C. Wesdemiotis, A. Fura, F.W. McLafferty, J. Am. Soc. Mass Spectrom. 2 (1991) 459.
[31] S. Beranova, C. Wesdemiotis, Int. J. Mass Spectrom. Ion Processes 134 (1994) 83.
[32] J.L. Holmes, Mass Spectrom. Rev. 8 (1989) 513.
[33] E. Kassab, E. Evleth, J. Am. Chem. Soc. 109 (1987) 1653.
[34] A. Demolliens, O. Eisenstein, P.C. Hiberty, J.M. Lefour, G. Ohanessian, S.S. Shaik, F. Volatron, J. Am. Chem. Soc. 111 (1989) 5623.
[35] A.I. Boldyrev, J. Simons, J. Chem. Phys. 97 (1992) 6621.
[36] B.A. Smart, C.H. Schiesser, J. Comput. Chem. 16 (1995) 1055.
[37] M.L. McKee, J. Phys. Chem. 97 (1993) 10971–10976.
[38] M. Gu, F. Tureček, J. Am. Chem. Soc. 114 (1992) 7146–7151.
[39] J.B. Foresman, M. Head-Gordon, J.A. Pople, M.J. Frisch, J. Phys. Chem. 96 (1992) 135.
[40] S. Kano, Y. Tanaka, E. Sugino, S. Hibino, Synthesis (1980) 695.
[41] F. Tureček, M. Gu, S.A. Shaffer, J. Am. Soc. Mass Spectrom. 3 (1992) 493.
[42] D.W. Kuhns, T.B. Tran, S.A. Shaffer, F. Turecek, J. Phys. Chem. 98 (1994) 4845.
[43] D.W. Kuhns, F. Turecek, Org. Mass Spectrom. 29 (1994) 463.
[44] M.J. Frisch, G.W. Trucks, H.B. Schlegel, P.M.W. Gill, B.G. Johnson, M.A. Robb, J.R. Cheeseman, T.A. Keith, G.A. Petersson, J.A. Montgomery, K. Raghavachari, M.A. Al-Laham, V.G. Zakrzewski, J.V. Ortiz, J.B. Foresman, J. Ci-

oslowski, B.B. Stefanov, A. Nanayakkara, M. Challacombe, C.Y. Peng, P.Y. Ayala, W. Chen, M.W. Wong, J.L. Andres, E.S. Replogle, R. Gomperts, R.L. Martin, D.J. Fox, J.S. Binkley, D.J. Defrees, J. Baker, J.P. Stewart, M. Head-Gordon, C. Gonzalez, J.A. Pople, GAUSSIAN 94 (Revision D.1), Gaussian, Inc., Pittsburgh, PA, 1995.
[45] F. Tureček, J. Phys. Chem. A 102 (1998) 4703.
[46] A.D. Becke, J. Chem. Phys. 98 (1993) 5648.
[47] S.H. Vosko, L. Wilk, M. Nusair, Can. J. Phys. 58 (1980) 120.
[48] C. Lee, W. Yang, R.G. Parr, Phys. Rev. B 37 (1988) 785.
[49] J.E. Szulejko, Revised Proton Affinity Scale, University of Waterloo, Waterloo, 1996.
[50] W.G. Mallard and P.J. Lindstrom (Eds.), NIST Chemistry Webbook, NIST Standard Reference Database, No. 69, March 1998; National Institute of Standards and Technology; Gaithersburg, MD.; http://webbook.nist.gov/chemistry.
[51] S.G. Lias, J.E. Bartmess, J.F. Liebman, J.L. Holmes, R.D. Levin, G.W. Mallard, J. Phys. Chem. Ref. Data, 17 (1988) (suppl. 1).
[52] W.L. Fitch, A.D. Sauter, Anal. Chem. 55 (1983) 832–835.
[53] F. Tureček, M. Gu, Org. Mass Spectrom. 27 (1992) 1335–1336.
[54] F. Tureček, J. Phys. Chem. A, submitted.
[55] M.T. Nguyen, S. Creve, L.G. Vanquickenborne, J. Phys. Chem. 100 (1996) 18422–18425.